Comparative study of various current controllers for the switched reluctance machine

Xavier Rain, Olivier Bethoux

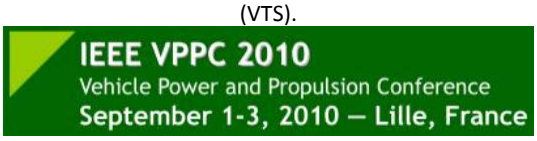

Accepted Manuscript

Comparative study of various current controllers for the switched reluctance machine

Xavier Rain, Mickael Hilairet and Olivier Bethoux

DOI: doi: 10.1109/VPPC.2010.5729145

Reference: VPPC 2010

Publisher: IEEE

To appear in: ***IEEE Conferences***

Conference date: 1-3 September 2010, Lille, France

Date of Publication: 10 March 2011 (available on line)

Please cite this article as:

X. Rain, M. Hilairet and O. Bethoux, "Comparative study of various current controllers for the switched reluctance machine", 2010 IEEE Vehicle Power and Propulsion Conference, Lille, 2010, pp. 1-6.

doi: 10.1109/VPPC.2010.5729145

URL:
http://ieeexplore.ieee.org/stamp/stamp.jsp?tp=&arnumber=5729145&isnumber=5728974

Document Version: Early version, also known as pre-print

Comparative study of various current controllers for the switched reluctance machine

Xavier Rain, Mickaël Hilairet, *member, IEEE,* Olivier Bethoux, *member, IEEE,*
Laboratoire de Génie Electrique de Paris (LGEP) / SPEE-Labs,
CNRS UMR 8507; SUPELEC; Université Pierre et Marie Curie P6; Université Paris-Sud 11;
11 rue Curie, Plateau de Moulon F91192 Gif sur Yvette CEDEX
Email: xavier.rain@orange.fr ; mickael.hilairet@lgep.supelec.fr ; olivier.bethoux@lgep.supelec.fr

***Abstract*— This paper presents three current control strategies for a switched reluctance machine (SRM). Two classical controllers are recall : the hysteresis and the proportional - integral controller. Dynamic and current ripples with both controllers are compared and discussed. Then, a new current controller qualified as "hybrid controller" is proposed. It is a combination of the two previous structures. The principle of this controller is detailed and its influence on the current control performance is described. The three strategies are first tested by simulation, and then on an experimental test bench.**

***Index Terms*— Switched reluctance machine, current control, hysteresis, linear controller, gain scheduling controller, hybrid controller, current ripples.**

I. Introduction

THE switched reluctance machine (SRM) had attracted many researchers over the last decade. This is certainly due to its numerous advantages such as simple and robust construction, high-speed and high-temperature performance, low costs, and fault tolerance control capabilities [1], [2].

The performance of SRM has been enhanced greatly due to advances in power electronics and computer science. Nowadays, SRM are under consideration in various applications requiring high performances such as in electric vehicle propulsion [3], [4], automotive starter-generators [1], [2] and aerospace applications [5], [6].

However, several disadvantages like acoustic noise generation, torque ripple, nonlinear electromagnetic characteristics and the strong dependence on the rotor position are limiting its utilization compared to other type of machines. The main limitation of the SRM are the acoustic noise generation and the nonlinear electromechanical behaviour (dependence on the current and mechanical position). Therefore, the design of an appropriate controller to achieve high performances must take into account this two phenomena's.

Several linear and nonlinear controllers that achieve high dynamic control can be found in a vast literature available on this topic. The most commonly used method to control the current in SRM is the hysteresis controller for its robustness, high dynamic range, easiness of implementation, and does not require any model of the system [7]. Its structure is very simple to implement and requires no knowledge of the electrical model of the machine, or special knowledge in automatic. However, this type of controller gives the disadvantage of variable switching frequency that may cause a subsonic noise in SRM [8]. An alternative solution is a fixed switching frequency operation (PWM) with linear and nonlinear controllers. Such controllers are widely used for variable speed/torque of AC machines. This technique makes the machine less sensitive to acoustic noise, but is in general less dynamic than a hysteresis regulator.

Several nonlinear control methods, such as the feedback linearizing [9], passivity [10], back-stepping [11] and sliding mode [12] have been applied to control the SRM. The speed control of SRM has been treated extensively in the literature while little research has been devoted to current controlling, witch constitutes the main part of the controller. In this article, three current control strategies are compared. Simulation and experimental results on a 8/6 SRM are detailed.

This paper is organized into four sections as follows: In the first section, the paper presents the SRM's current control. Then, in the next two sections, it describes and compares the hysteresis and proportional-integral controllers. Finally, the advantages of these latter are associated to design an "hybrid controller" that is described in section V.

II. SRM's current controller

Fig.1 describes a SRM's speed control strategy based on an average torque control [13].

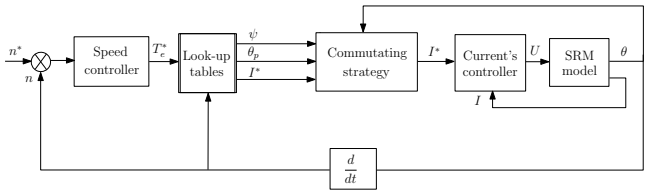

Fig. 1. SRM's architecture control

As with any type of electrical machine speed controlled, the speed controller's (Integral-Proportional) output defined the electromagnetic required torque T_e^*. In this strategy, the reference torque is considered as an average torque over on conducting period. It is controlled indirectly by adjusting the three fundamental variables, ie., reference phase current I^*, turn-on angle ψ, and conduction period θ_p. One important feature of this classical controller is that the reference phase current is constant over one excitation period. Thereby, this

control is also called “square wave control”. Many combinations of these control variables are possible to operate the SRM drive at one specific torque-speed operating point. However, one suitable combination for one speed-torque operating point should be chosen, based on the desired optimization goal, e.g., efficiency or low torque ripple [13]. Using simulations, an optimal set of the control variables over the entire operating range can be obtained. The torque translation into a current reference is located in a look-up table. Linear data interpolation is performed on-line to compute the optimal control parameters depending on the operating point. Many classical SRM torque controllers use this approach and rely on look-up tables of the control parameters.

Fig. 2 presents a continuous model of the SRM’s current control. Simulation and experiment show that it is necessary to add a back-emf compensation, which acts as a strong disturbance dynamics. The back-emf $\hat{E}$ is estimated from an analytical model of the phase’s inductance L, dependent to the current and rotor position [14].

The simulation requires an electric model for each SRM’s phase. The phase electric model is derived from the classical equation:

$$U = R\,i + \frac{d\Phi(i,\theta_e)}{dt}$$

where R is the phase’s resistance and Φ is the phase’s magnetic flux. The magnetic flux depends on the current and the electric position θ_e of the rotor (angle between a rotor tooth and the phase’s unaligned position). Therefore, a look-up table (performed off-line) give the phase’s current from the flux and the position. It is obtained by FEA [15].

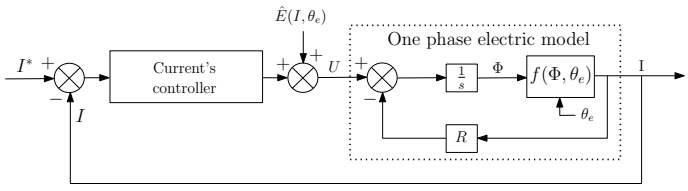

Fig. 2. SRM’s current control

III. Hysteresis controller

The most classical and easiness implemented controller is the hysteresis. The only control parameter is the hysteresis band ΔH. In the case of an analog implementation, this parameter ensures that the instantaneous current is bounded between $i^* \pm \Delta H/2$, where i^* is the desired current. In this case, the current ripple is equal to ΔH and the current controller output takes only two distinct values $\pm U_{dc}$.

The two main drawbacks of this controller are the increase of the current ripples at steady state and the production of a variable switching frequency, which generate additional acoustic noise in SRM. To reduce these ripples, the hysteresis band ΔH must be reduced but it increase the switching frequency of the converter, and therefore increase the power converter losses.

However, in practice, the current controller is implemented on a processor. To reduce these ripples as much as possible, the sample time T_s must be small. Therefore, this latter is limited according the processor capacities. Here, a 1103 Dspace board is used on the test bench, that limit the sample time at $50\,\mu$s. Thereby, the ripple current Δi can be evaluated as:

$$\Delta i \approx \frac{N\,T_s\,|U_{dc} - R\,i - E|}{L_{inc}}$$

where, N is the number of consecutive sample times where a constant voltage is applied to the phase, U_{dc} is the supply voltage of the converter (here U_{dc} = 24 V), R the phase’s resistance, E is the back-emf, and L_{inc} is the phase’s incremental inductance.

Fig. 3.a and 3.b shows the current and voltage in one phase of the SRM, for a reference current equal to 30 A, that produce an average electromagnetic torque T_{em} equal to 3,7 N.m, at 500 rpm. The hysteresis band is set to zero.

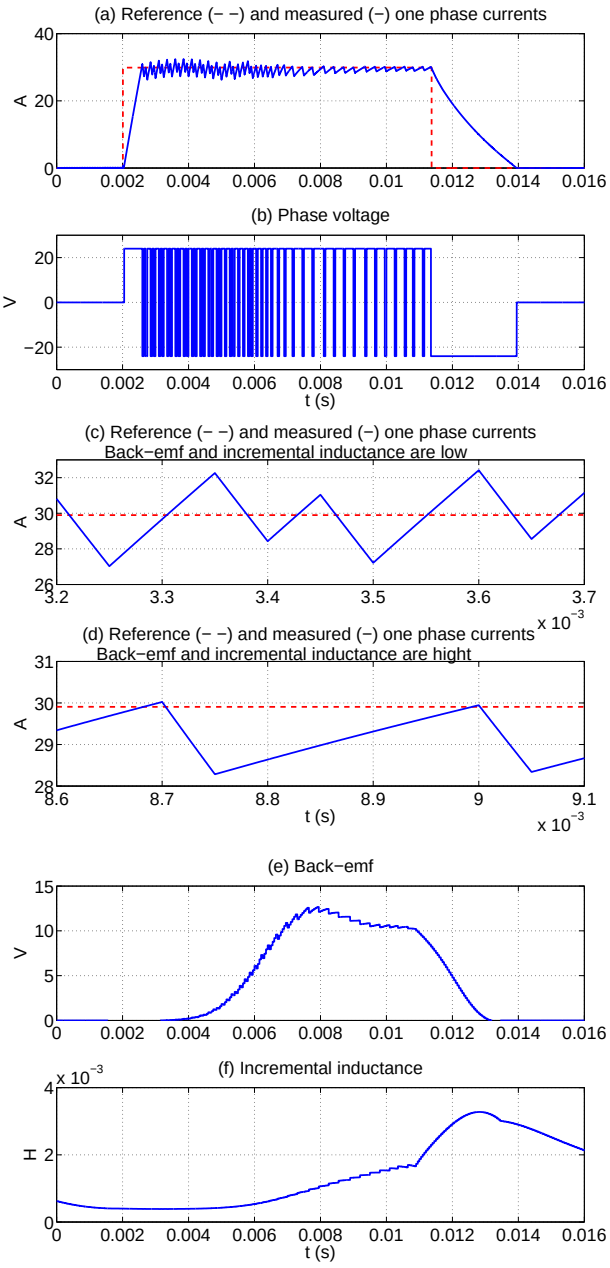

Fig. 3. Simulation result : instantaneous current and voltage phase, back-emf and incremental inductance - Hysteresis controller.

It appears that the current can move in one direction during several sampling periods, and especially when the back-emf and the incremental inductance are high (see Fig. 3.d, e, f). The instantaneous current can exceeded the defined bandwidth ΔH du to the high sample time. From Fig. 3.c, the maximal current ripples are evaluated of about 6A. The discretized control causes a current witch is not centred with the reference. Therefore, the static error is not zero.

An experimental test has been performed with the same operating point as the simulation one: T_{em} = 3,7 N.m, 500 rpm and ΔH is set to zero. Fig. 4 shows the current and it's reference in one phase, and the voltage applied to the SRM's phase. The experimental results are similar to the simulation's one. The maximum current ripple is about 5A.

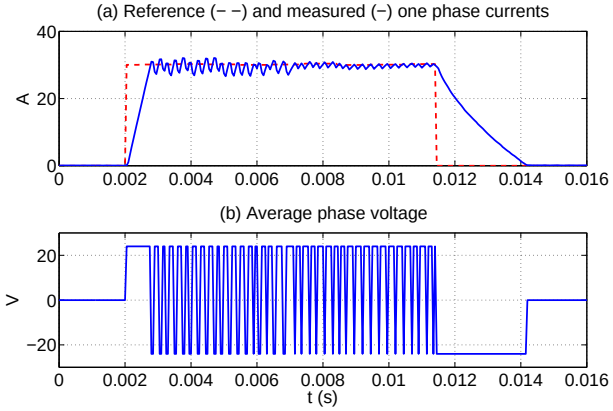

Fig. 4. Experimental result : instantaneous current and voltage phase - Hysteresis controller.

To reduce these ripples, the sampling period must be reduced, which is impossible with the 1103 Dspace board. In order to improve the hysteresis controller implementation, this latter must be made at a hardware level, using an analog controller or a FPGA. However, the hysteresis current controller can be replaced by a linear or non linear controller with a constant chopping frequency, so as to keep a software implementation.

IV. Proportional - integral controller

A. Introduction

Many linear and non-linear controllers using PWM can be adopted to control the current [9] [10] [11] [12]. In this work, a proportional - integral controller is implemented. Fig. 5 shows the blok diagram of this current controller associated with a SRM's phase model, where U is the average reference voltage applied to a phase. Indeed, unlike a conventional machine, the back-emf E can be seen as a disturbance for the current control, that depends on $\partial L/\partial\theta_e$, where θe is the electrical position of the rotor. A compensation of the back-emf improve the current control. In practice, the controller is implemented on a processor. Fig. 6 shows the discrete PI controller.

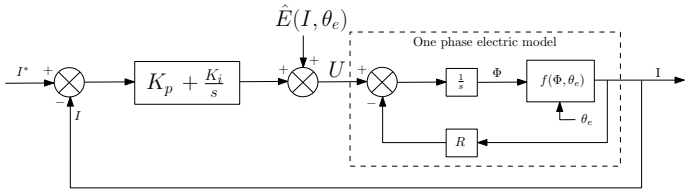

Fig. 5. Blok diagram of the current PI controller.

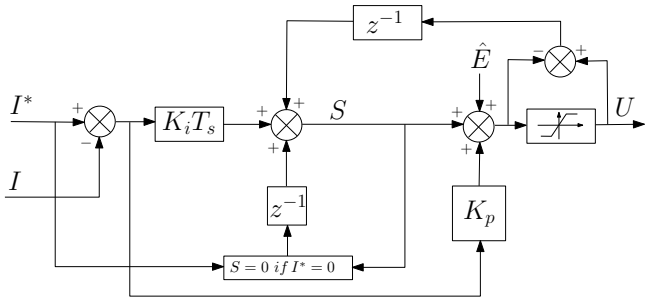

Fig. 6. Blok diagram of the discreet PI controller.

The integrator is approximed by a Euler's integral: $S_k = S_{k-1} + K_i\,T_s$. This scheme includes two important elements:

- An anti-wind-up action, placed at the output of the controller to limit the output voltage to a maximum value depending on the characteristics of the machine and the static converter (24 V in our case).
- An initialization blok of the integrator when the current set point reverts to zero.

B. Controller design

If the compensation of the back-emf is ideal, the transfer function of the closed loop is:

$$\frac{I(s)}{I^*(s)} = \frac{\frac{K_p}{L_{inc}}\,s + \frac{K_i}{L_{inc}}}{s^2 + \left(\frac{K_p+R}{L_{inc}}\right)s + \frac{K_i}{L_{inc}}}$$

wich is identified with a second order system:

$$\frac{I(s)}{I^*(s)} = \frac{2\,\xi\,\omega_n\,s + \omega_n^2}{s^2 + 2\xi\omega_n s + \omega_n^2}$$

This leads to:

$$\begin{aligned} K_i &= L_{inc}\,\omega_n^2 \\ K_p &= 2\,\xi\,L_{inc}\,\omega_n - R \end{aligned}$$

where ω_n is the bandwidth and ξ the damping coefficient.

If the regulator's gains are constants, the current's dynamics is not fixed, and is not optimal. Given that the phase's inductance of the SRM depends on the electrical position and current, the idea is to compensate these variations, to ensure a fixed dynamics of the closed loop. The gain's adaptation is based on an analytical model of the inductance. In [16], an improvement of the current control associated with a torque ripple reduction compared to a classical PI controller with fixed gains has been shown.

Variable gains leads to a fixed closed-loop dynamic, so that the bandwidth ω_n and the damping coefficient ξ remains constant. A optimum value of the stability margin has been obtained for ξ = 0,707 and ω_n = 6000 rad/s [16].

Fig. 7 shows a simulation test with the proportional - integral controller with variable gains. As expected, the current

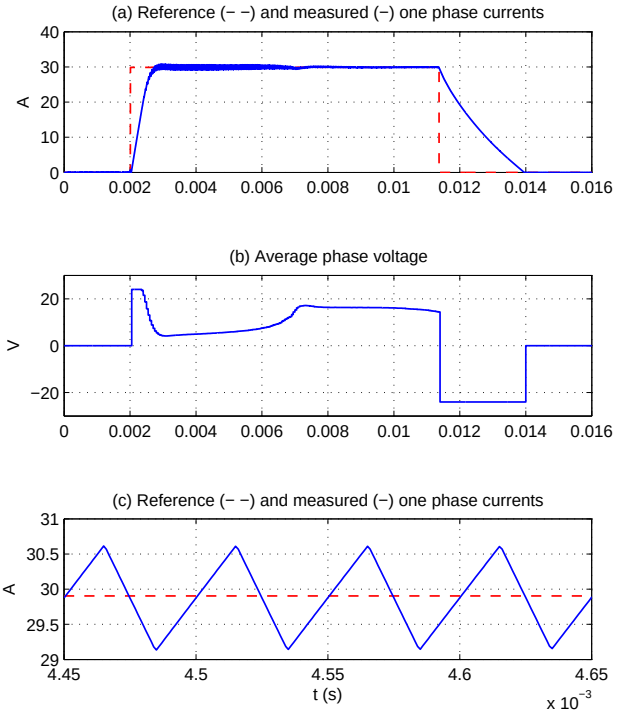

Fig. 7. Simulation result: instantaneous current and average voltage phase with variable-gains PI controller.

ripple is reduced. The switching frequency of the power converter is equal to the algorithm sampling frequency, and is set to 20 kHz. As for the hysteresis, the current ripple is important at the unaligned position, and is nearly equal to 1/4 of the current ripple with the hysteresis controller (see Fig. 7.c). Indeed, we have:

$$\Delta I = \frac{T_s\,(U_{dc} - R\,i)}{2\,L_{inc}} = 1,45\,A$$

Fig. 8 shows an experimental result with the variable-gains PI controller. Simulation and experimental results are similar. The acoustic noise is appreciable reduce with such controller.

Simulation and experimental results show that the hysteresis

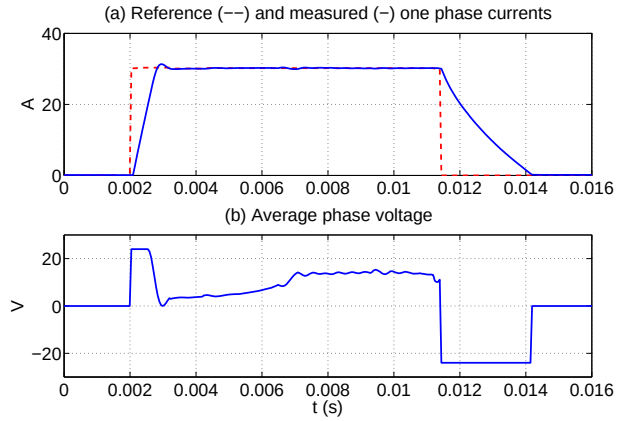

Fig. 8. Experimental result: instantaneous current and average voltage phase with variable-gains PI controller.

response time for a current step is the main advantage of this latter compared to the PI controller response time (here, the current settle in 0,8 ms with the hysteresis, and in 1,2 ms with the variable-gains PI). On the other hand, the behaviour of the PI controller is more smooth in steady state. Both controllers have some advantages and drawbacks. Therefore, one idea consist on merging the main advantages of the two controllers, in a so called "hybrid controller".

V. Hybrid controller

A. Presentation

As stated before, both controllers have some advantages and drawbacks. The hysteresis controller is well suited during transients for its high dynamic; and the PI controller (linear and non-linear controllers in general) is appreciable at steady state. Therefore, one idea consist on merging the main advantages of the two controllers, in a so called "hybrid controller".

Fig. 9 represents the current response that is composed of three parts:

- First part (mode 1): a current range $2\,\Delta I$ centred around the reference current I^* is defined. If the current is outside this region, it is the hysteresis controller that is engaged in the current control. Therefore, the phase voltage are equal to $\pm U_{dc}$.
- Second part (mode 2): if the current is in the interval $2\,\Delta I$, the current control is made by the PI controller with fixed gains. In the case of the hybrid controller, a PI controller with variable gains seems not justified.
- Third part (mode 0): in this case, the current reference is equal to zero. The voltage applied to the SRM is equal to $-U_{dc}$ as long as the current is not zero. Later, the voltage is equal to zero.

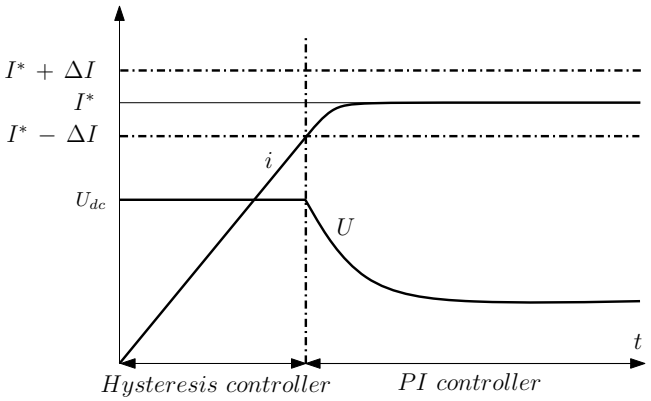

Fig. 9. Principle of the hybrid controller.

In order to avoid discontinuity during transitions between the first mode and second mode (and *vice versa*), the integrator of the PI controller must be initialized to the value $S = U_{dc} - K_p\,\Delta I$.

Fig. 10 illustrates a simulation test with the hybrid controller. The hybrid controller uses the linear controller when the instantaneous current is near to the reference. It is sufficient to use a PI controller with constant gains without degradation of dynamic, since the reference current is almost constant.

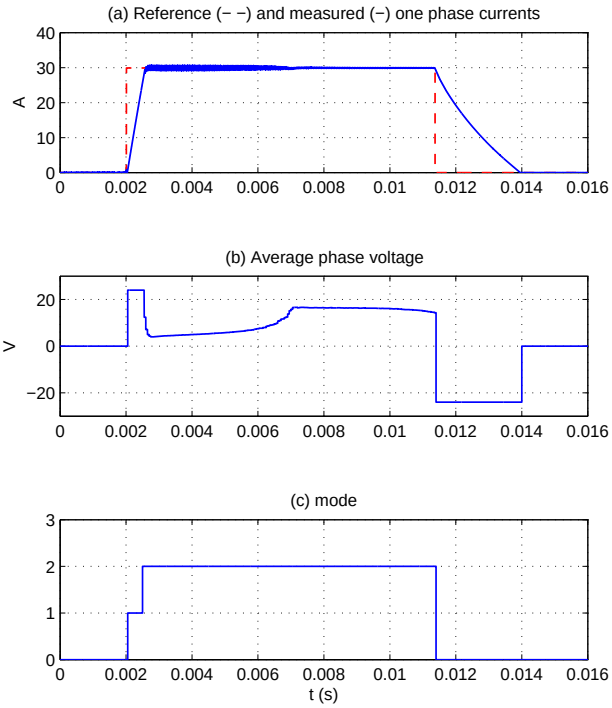

Fig. 10. Simulation result: instantaneous current and average phase voltage with hybrid controller.

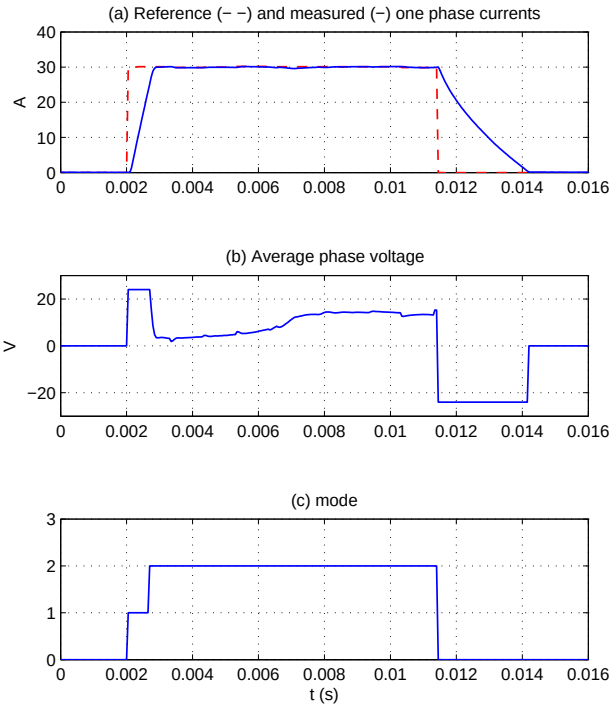

Fig. 11. Experimental result: instantaneous current and average phase voltage with hybrid controller.

Moreover, the gains can be reduced, in order reduce the controller dynamic and therefore the controller sensitivity to measurement noise. The PI controller gains are set to K_p = 6, K_i = 20000 and, in order to avoid overshoots, ΔI is set to 6 A.

The transition between the first mode to the second one is obtained when the current is equal to 24 A (I^* = 30 A). The variable "mode" indicates this transition (1 $\Rightarrow$ 2). At the transition, the controller output voltage U is maximum: $U = U_{dc}$, which provides the maximum current dynamic. The statement shows that the dynamics of the hybrid controller is as good as the hysteresis one, while reducing the current ripples. This controller thus combines the advantages of the previous two controllers. It is therefore very effective.

Fig. 11 illustrates an experimental test with the hybrid controller. The PI controller gains are set to K_p = 6, K_i = 20000 and ΔI is set to 6 A. This experimental results shows that the dynamic has been improved compared to the PI controller with variable gains while maintaining the PI advantages at steady state.

B. Robustness tests

Several simulation tests for testing the robustness issue with respect to parameter variations have been performed. First, the influence of the parameter ΔI is analysed (see Fig. 12 and 13).

Fig. 12 shows the current response when ΔI is too low. ΔI is set to 1 A. There are commutations between mode 1 and 2. That leads to an additional current ripple due to the discrete hysteresis controller. Thereby, ΔI should not be too low.

Fig. 13 shows the current response when ΔI increase. ΔI is set to 25 A. There is an increase of 25 % on the response time. Thereby, ΔI should not be too high.

An other simulation test has been realized by considering a $\pm 30\%$ variation of the phase's magnetic flux (equivalent to an inductance variation at constant current). Fig. 14 indicates that the current response is not very affected by this parametric uncertainties. The average phase voltage is modified to have a similar response.

Finally, a simulation test has been performed to show the influence of the speed on the controller's performance. Speed is set to 1000 rpm. Fig. 15 shows the good robustness of the controller against a speed variation, mainly du to the back-emf compensation.

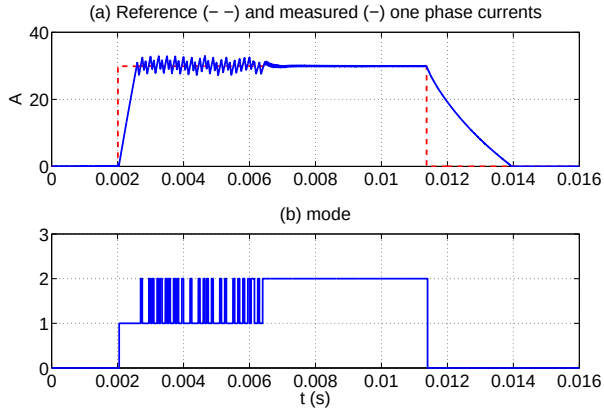

Fig. 12. Simulation result: hybrid controller with ΔI = 1 A.

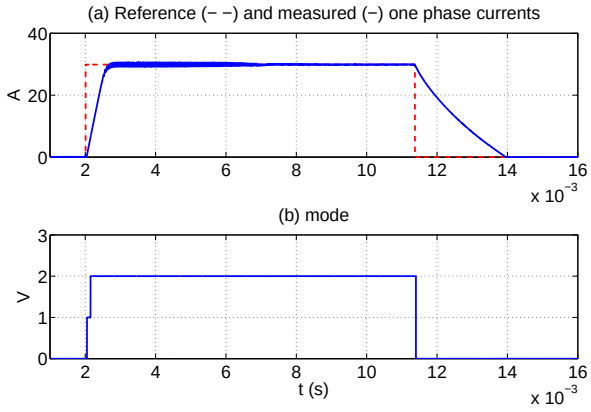

Fig. 13. Simulation result: hybrid controller with ΔI = 25 A.

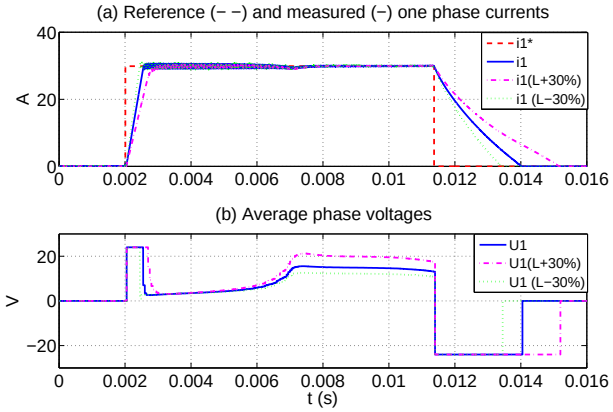

Fig. 14. Simulation result: instantaneous currents and average phase voltages for an inductance variation at 500 rpm.

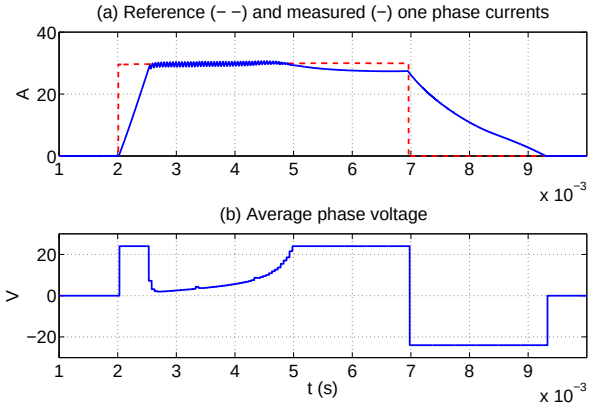

Fig. 15. Simulation result: instantaneous currents and average phase voltages at 1000 rpm.

VI. Conclusion

A new current controller for the SRM is proposed. It is an association of an hysteresis and proportional - integral controller. Therefore, it combines the advantages of these latter, high dynamics, low current ripples and good robustness. The proposed controller has been validated by simulation and experimentally. The results are satisfactory and proved the feasibility of this new type of controller.

TABLE I

Prototype characteristics

Geometric parameters			
Number of rotor poles	6	Stator pole arc	19.8°
Number of stator poles	8	Rotor pole arc	20.65°
Stator outer diameter	143 mm	Airgap lebgth	0.8 mm
Shaft diameter	23 mm		
Electrical parameters			
Number of phases	4	Nominal speed	3000 rpm
Nominal power	1.2 kW	Nominal voltage	24 V
Phase's resistance	$50\,m\Omega$		

References

[1] B. Fahimi, A. Emadi, R.B. Sepe, "A switched reluctance machine-based starter/alternator for more electric cars," *IEEE Industry Applications Magazine*, Vol. 20, no 1, pp. 116-124, Mar. 2004.

[2] J. Faiz, K. Moayed-Zadeh, "Design of switched reluctance machine for starter/generator of hybrid electric vehicle," *Electric Power Systems Research, Elsevier*, Vol. 75, no 2-3, pp. 153-160, 2005.

[3] B.A. Kalan, H.C. Lovatt, G. Prout, "Voltage control of switched reluctance machines for hybrid electric vehicles," *IEEE Power Electronics Specialists Conference (PESC'02)*, Vol. 4, pp. 1656-1660, 2002.

[4] M. Krishnamurthy, C.S. Edrington, A. Emadi, P. Asadi, M. Ehsani, B. Fahimi, "Making the case for applications of switched reluctance motor technology in automotive products," *IEEE Transactions on Power Electronics*, Vol. 21, pp. 659-675, May 2006.

[5] R.T. Naayagi, V. Kamaraj, "Shape optimization of switched reluctance machine for aerospace applications," *31st Annual Conference of IEEE Industrial Electronics Society (IECON'05)*, Nov. 2005.

[6] A.V. Radun, "High-power density switched reluctance motor drive for aerospace applications," *IEEE Transactions on Industry Applications*, Vol. 28, no 1, pp 113-119, 1992.

[7] M.R. Benhadria, K. Kendouci, B. Mazari, "Torque Ripple Minimization of Switched Reluctance Motor Using Hysteresis Current Control," *IEEE International Symposium on Industrial Electronics ISIE'06*, Vol. 3, pp. 2158-2162, Jul. 2006.

[8] F. Blaabjerg, P.C. Kjaer, P.O. Rasmussen, C. Cossar, "Improved digital current control methods in switched reluctance motor drives," *IEEE Transactions on Power Electronics*, Vol. 14, no 3, pp. 563-572, may 1999.

[9] G.S. Buja, R. Menis, M.I. Valla, "Variable structure control of an SRM drive," *IEEE, Transactions on Industrial Electronics*, Vol. 40, no 1, pp. 56-63, Feb 1993.

[10] G. Espinosa-Perez, P. Maya-Ortiz, M. Velasco-Villa, H. Sira-Raminez, "Passivity-based control of switched reluctance motors with nonlinear magnetic circuits," *IEEE Transactions on Control Systems Technology*, Vol. 12, no 3, pp. 439-448, may 2004.

[11] M.T. Abrifai, J.H. chow, D.A. Torrey, "Practical application of backstepping Nonlinear current control to a switched-Reluctance motor," Proceedings of the American Control Conference, Vol. 17, no 6, pp. 1306-1317, Chicago, Illinoi, 2009.

[12] H. Yang, S.K. Panda, Y.C. Liang, "Experimental investigation of feedback linearization controller for switched reluctance motor," Power Electronics Specialists conference, Vol. 2, pp. 1804-1810, Jun. 1996.

[13] H. Hannoun, M. Hilairet, C. Marchand, "Comparison of instantaneous and average torque control for a Switched Reluctance Motor," *IEEE International Symposium on Industrial Electronics ISIE*, Jun. 2008.

[14] H. Hannoun, M. Hilairet, C. Marchand, "Analytical modeling of switched reluctance machines including saturation," *IEEE International Electric Machines and Drives Conference IEMDC*, May. 2007.

[15] M. Besbes, B. Multon, "MRVSIM Logiciel de simulation et d'aide à la conception de Machines à réluctance variable à double saillance à alimentation électronique," Dépôt APP CNRS en 2004, n°IDDN.FR.001.430010.000.S.C.2004.000.30645

[16] H. Hannoun, M. Hilairet, C. Marchand, "Design of an SRM speed control strategy for a wide range of operating speeds," *IEEE Transactions on Industrial Electronics*, Vol. 57, no 9, Sept. 2010.